IEEE Access
Multidisciplinary ⋮ Rapid Review ⋮ Open Access Journal

Received 28 July 2023, accepted 28 August 2023, date of publication 4 September 2023, date of current version 8 September 2023.

Digital Object Identifier 10.1109/ACCESS.2023.3311714

RESEARCH ARTICLE

Adaptive Neural Backstepping Control for Harmonic Drive System Based on Modified LuGre Friction Model

YU XIA[1], (Graduate Student Member, IEEE), CHENG WANG[1], YANKUI SONG[1], JIANLIN CAI[1], AND GONG CHENG[2]

[1]State Key Laboratory of Mechanical Transmission, Chongqing University, Chongqing 400044, China
[2]School of Mechanical Engineering and Automation, Chongqing Industry Polytechnic College, Chongqing 401120, China

Corresponding author: Gong Cheng (chenggong@cqipc.edu.cn)

This work was supported by the Aeronautical Science Foundation of China under Grant 202000020Q9001.

ABSTRACT To improve the control accuracy and stability of the harmonic drive system under the influence of nonlinear friction and external disturbances, we have developed an adaptive neural backstepping control approach with friction compensation. During the design process, we employ a nonlinear observer based on a novel modified LuGre model with friction compensation. This observer effectively reduces the influence of nonlinear friction on the harmonic drive system, even under dynamic changes in the environment. Additionally, we utilize a Chebyshev neural network to approximate unknown disturbances applied to the harmonic drive system. To prevent violations of output constraints, we introduce a tangent barrier Lyapunov function. Furthermore, to address the challenges of ''explosion of complexity'' and poor precision associated with first-order filters in backstepping, we integrate the inverse hyperbolic sine function tracking differentiator into this controller. Finally, we employ the Lyapunov criterion to prove that all errors in the closed-loop system are uniformly bounded. Simulation results confirm the feasibility of the proposed control scheme and demonstrate better closed-loop behavior compared to that obtained using a radial basis function dynamic surface controller.

INDEX TERMS Adaptive neural backstepping control, Chebyshev neural network, harmonic drive system, modified LuGre model, tangent barrier Lyapunov function.

I. INTRODUCTION

The harmonic drive (HD) system is widely utilized in various fields such as aerospace and industrial robotics due to its compact structure, high transmission ratio, smooth operation, and high efficiency [1], [2]. However, the HD system faces challenges caused by the intricate sliding friction contact between the wave generator and the inner wall of the flexible wheel, as well as between the teeth of the flexible wheel and the teeth of the rigid wheel [3], [4]. These factors contribute to strong nonlinear friction throughout the reducer, which in turn makes the system sensitive to unknown external disturbances. Therefore, there is immense theoretical significance and practical value in studying the dynamic characteristics of the HD system and devising effective control strategies to achieve precise compensation for nonlinear friction and external disturbances.

The LuGre friction model is widely used in model-based friction compensation of control systems due to its ability to accurately describe various dynamic and static characteristics of nonlinear friction, including presliding displacement, frictional lag, and varying break-away force [5]. In LuGre-model-based friction compensation, the primary control scheme involves an adaptive control method based on an observer, which estimates the unmeasurable state variables of the LuGre model [6]. Various control methods have been proposed in this context. For example, an iterative learning control method based on a dual-observer is presented to ensure that the tracking error converges to zero in the $L2$-norm sense [7]. An adaptive control method based on a projection

The associate editor coordinating the review of this manuscript and approving it for publication was Jinquan Xu.

observer is introduced to achieve asymptotic tracking [8]. Another adaptive control method employs an observer with filtered states to guarantee that the tracking error converges to zero under a persistent excitation condition for the dynamical function of friction [9]. Additionally, adaptive control methods based on neural networks [10] and parameter identification [11] are also commonly employed for LuGre-model-based friction compensation. The aforementioned control methods primarily address the issues of asymptotic tracking [7], [8], [9] when the exact values of parameters in the dynamic equation of the LuGre model are known, or approximate tracking [10], [11] when all parameters of the LuGre model are unknown. However, they overlook the dynamic changes of these parameters under varying external conditions. Therefore, a new focus of research is to develop better approaches for describing the dynamic behavior of the LuGre model.

Friction compensation using modified LuGre models has been extensively studied by researchers. For instance, an adaptive robust controller based on a modified LuGre friction observer is proposed for uncertain linear motors to ensure a sufficiently small tracking error [12]. By utilizing the modified LuGre model, the vector field of the friction equation becomes zero when the speed exceeds a preset limit, leading to improved dynamic friction compensation across a wide range of velocity regulation. Building upon this, another modified LuGre model combined with a zero-velocity crossing window is proposed to address lag and model oscillation in force control systems [13]. Other modification methods, such as those based on function-based approximation theory, replace the non-smooth LuGre model with a smooth friction model [14]. Interested readers can find more information in [14], [15], and [16]. While the aforementioned modified LuGre models with friction compensation enhance dynamic friction performance to some extent, most of them do not explicitly consider the influence of external disturbances.

The backstepping control (BC) framework, an adaptive control technique, is a powerful strategy for nonlinear servo systems under nonlinear friction and external disturbance conditions. Unlike the sliding-mode control (SMC) framework [17], which suffers from internal chattering that limits its expansion, BC has been proven to overcome this limitation [18]. Additionally, incorporating specific control tools in the controller design process can significantly enhance controller performance. Dynamic surface control (DSC) technology [19] addresses the ''explosion of complexity'' in adaptive backstepping control of high-order nonlinear systems by introducing a first-order filter (FOF) into the BC framework. While the FOF can eliminate the drawbacks of BC, its accuracy is often low. To compensate for this, a tracking differentiator (TD) [20] is employed to achieve higher precision. Neural networks (NNs) [21], [22], [23], [24] are widely utilized in controller design because they can approximate unknown smooth functions with arbitrary precision. Common types include radial basis function (RBF) neural networks and fuzzy basis function (FBF) neural networks. Furthermore, when combined with DSC, radial basis function dynamic surface control (RBFDSC) and fuzzy basis function dynamic surface control (FBFDSC) exhibit notable advantages in solving practical control problems. However, these NNs often require additional parameters, prior knowledge of approximation functions, and real-time parameter updates. In contrast, the Chebyshev neural network [25] offers significant advantages as its inputs only rely on a subset of Chebyshev polynomials. In practical applications, the harmonic drive (HD) system often needs to consider output constraint issues. A barrier Lyapunov function (BLF) [26], proposed for constraint handling in nonlinear systems, is introduced due to its property of approaching infinity when its arguments approach certain limits. Previous works on BLF typically employ logarithmic BLF (BLF-Log) to design control systems [27]. However, if the constraint of the initial error approaches convergence to zero, BLF-Log will also converge to zero and replace the quadratic form. Considering practical needs and theoretical challenges, constructing the BLF-tan for the HD system is more appropriate.

Based on our current understanding, the combination of adaptive BC, NN, TD, and BLF has not been previously applied to control the friction compensation of the HD system. Consequently, in this paper, an adaptive neural backstepping control (ANBC) scheme is designed specifically for the HD system. The main contributions of this paper are given as follows:

1. The proposed ANBC scheme in this paper combines the Chebyshev neural network, Inverse Hyperbolic Sine Function Tracking Differentiator (IHSFTD), Tangent Barrier Lyapunov Function (TBLF), and minimum learning parameters. Compared to other neural networks [21], [22], [23], [24], the Chebyshev neural network can approximate unknown functions without the need to determine the centers of the basis functions. This simplifies the network structure and training process, making it more efficient. The IHSFTD is preferred over FOF [19] as it provides a higher accuracy in estimating the virtual input derivative. This improves the overall performance of the control system, especially in accurately tracking the system dynamics. In terms of BLF, the TBLF used in this study exhibits a wider applicability compared to other types [27]. The TBLF can handle a broader range of constraints, making it suitable for a variety of control scenarios.
2. The ANBC scheme proposed in this paper is built upon a novel modified LuGre model. One notable advantage of this model is the ability to anticipate the effects of nonlinear friction in advance. By introducing only two adaptive parameters, the influence of external uncertainties on friction compensation can be mitigated. In traditional approaches [12], [13], [14], [15], [16], the consideration of nonlinear friction and the reduction of uncertainties in friction compensation typically require more complex models

and a larger number of adaptive parameters. The modified LuGre model used in the ANBC scheme simplifies the control process while still accounting for the influence of nonlinear friction and reducing the impact of external uncertainties.

This paper is organized in the following manner. Section II states system formulation and preliminaries. In Section III, the design of the ANBC is given, and the stability analysis is executed. Then, in Section IV, simulation analyses are given. Finally, the conclusion is given in Section V.

II. SYSTEM FORMULATION AND PRELIMINARIES

A. SYSTEM DYNAMIC MODEL

Considering the influence of nonlinear factors such as flexible deformation, nonlinear friction, and unknown external disturbances, a second-order nonlinear dynamic model can be established for HD mechanisms [28], as described in equation (1).

$$\begin{cases} J_l\ddot{q}_l + c_l\dot{q}_l + F_f\left(\dot{q}_l\right) - K\left(q_m/N - q_l\right) + d_l = 0 \\ J_m\ddot{q}_m + c_m\dot{q}_m + (K/N)\left(q_m/N - q_l\right) + d_m = u \end{cases} \tag{1}$$

where $F_f\left(\dot{q}_l\right)$ denotes the nonlinear friction torque, J_l, c_l, d_l are the rotational inertia, the damping coefficient, and the unknown external disturbance of the driving mechanism, J_m, c_m, d_m are the rotational inertia, the damping coefficient and the unknown external disturbance of the motor, K represents the flexible stiffness, N denotes the reduction ratio of the reducer component, $q_l, \dot{q}_l, \ddot{q}_l$ denote the displacement, speed and acceleration of the drive mechanism respectively, $q_m, \dot{q}_m, \ddot{q}_m$ represent the displacement, angular speed and angular acceleration of the motor respectively, and u is the output torque of the motor.

The nonlinear friction force $F_f\left(\dot{q}_l\right)$ in the system (1) can be described by the LuGre friction model as

$$\begin{cases} F_f = \sigma_0 z + \sigma_1\dot{z} + \sigma_2\dot{q}_l \\ \dot{z} = \dot{q}_l - \left|\dot{q}_l\right| z/g\left(\dot{q}_l\right) \\ \sigma_0 g\left(\dot{q}_l\right) = F_c + \left(F_s - F_c\right) e^{-\left(\dot{q}_l/\dot{q}_s\right)^2} \end{cases} \tag{2}$$

where $\sigma_0, \sigma_1, \sigma_2$ is the stiffness coefficient, the damping coefficient and the viscous friction coefficient of the bristles in contact surface, z denotes the average deflection of bristles, $g\left(\dot{q}_l\right)$ represents bounded function, q_s is the Stribeck angular speed, F_c denotes the Coulomb friction, F_s denotes the stiction force.

In model (2), for the convenience of calculation, the coefficients $\sigma_0, \sigma_1, \sigma_2$ are usually regarded as constants. However, in actual working conditions, the coefficients σ_0, σ_1 will vary with the contact of the micro convex body and the proportion of load the oil film bears, and the coefficient σ_2 will be affected by the changes in the relative velocity and the temperature. Therefore, in order to more accurately reflect changes in internal friction of the reducer with the external environment, parameters ω and υ were introduced to improve the classical LuGre friction model. Then, the modified LuGre model can be expressed as

$$F_f = \omega\left(\sigma_0 z + \sigma_1\dot{z}\right) + \upsilon\sigma_2\dot{q}_l \tag{3}$$

In the equation (3), ω is used to reflect changes the average deflection of bristles. υ is used to reflect changes in the coefficient of viscous friction. They meet $0 < \omega_{\min} < \omega < \omega_{\max}$ and $0 < \upsilon_{\min} < \upsilon < \upsilon_{\max}$.

Substituting equation (3) into equation (2) yields

$$\begin{cases} F_f = \omega\left(\sigma_0 z + \sigma_1\dot{z}\right) + \upsilon\sigma_2\dot{q}_l \\ \dot{z} = \dot{q}_l - \left|\dot{q}_l\right| z/g\left(\dot{q}_l\right) \\ \sigma_0 g\left(\dot{q}_l\right) = F_c + \left(F_s - F_c\right) e^{-\left(\dot{q}_l/\dot{q}_s\right)^2} \end{cases} \tag{4}$$

Then, assuming that the actual LuGre model can be represented as

$$\begin{cases} \overline{F}_f = \omega\left(\overline{\sigma}_0 z + \overline{\sigma}_1\dot{z}\right) + \upsilon\overline{\sigma}_2\dot{q}_l \\ \dot{z} = \dot{q}_l - \left|\dot{q}_l\right| z/g\left(\dot{q}_l\right) \\ \overline{\sigma}_0 g\left(\dot{q}_l\right) = \overline{F}_c + \left(\overline{F}_s - \overline{F}_c\right) e^{-\left(\dot{q}_l/\bar{\dot{q}}_s\right)^2} \end{cases} \tag{5}$$

where $\overline{\sigma}_0, \overline{\sigma}_1, \overline{\sigma}_2, \overline{F}_c, \overline{F}_s, \overline{F}_f, \bar{\dot{q}}_s$ are the actual value of $\sigma_0, \sigma_1, \sigma_2, F_c, F_s, F_f, \dot{q}_s$.

However, the actual values of these parameters are difficult to obtain. If their nominal values are used to represent the actual model, equation (1) can be rewritten as

$$\begin{cases} J_l\ddot{q}_l + c_l\dot{q}_l + F_f\left(\dot{q}_l\right) - K\left(q_m/N - q_l\right) + \Delta + d_l = 0 \\ J_m\ddot{q}_m + c_m\dot{q}_m + (K/N)\left(q_m/N - q_l\right) + d_m = u \end{cases} \tag{6}$$

where $\Delta = \overline{F}_f\left(\dot{q}_l\right) - F_f\left(\dot{q}_l\right)$.

Define the system state variables $x_1 = q_l, x_2 = \dot{q}_l, x_3 = q_m, x_4 = \dot{q}_m$. Then the dynamic equation (1) is rewritten as follows

$$\begin{cases} \dot{x}_1 = x_2 \\ \dot{x}_2 = (1/J_l)\left[-c_l x_2 - F_f\left(x_2\right) + K\left(x_3/N - x_1\right) - d_l\right] \\ \dot{x}_3 = x_4 \\ \dot{x}_4 = (1/J_m)\left[u - c_m x_4 - (K/N)\left(x_3/N - x_1\right) - d_m\right] \end{cases} \tag{7}$$

For any given continuous signal x_{1d}, the four dynamics surfaces are defined as

$$\begin{cases} e_1 = x_1 - x_{1d} \\ e_2 = x_2 - \alpha_2 \\ e_3 = x_3 - \alpha_3 \\ e_4 = x_4 - \alpha_4 \end{cases} \tag{8}$$

where $\alpha_i, i = 2, 3, 4$ is the virtual control inputs.

Control Goal: All the signals of the closed HD system are uniform and ultimately bounded with the output position signal x_1 is restricted in the set $\Omega = \{x_1 \in \mathbb{R} \,||x_1| < a, \forall t > 0\}$.

Assumption 1: The reference trajectory x_{1d} is bounded by $-d \leq x_{1d} \leq d, (a > d > 0)$, and the time derivatives $\dot{x}_{1d}, \ddot{x}_{1d}$ are bounded.

B. INVERSE HYPERBOLIC SINE FUNCTION TRACKING DIFFERRENTIATOR

In order to avoid the explosion of complexity in the controller design, the tracking differentiator based on inverse hyperbolic sine function is introduced [29], which is expressed as

$$\begin{cases} \dot{v}_1(t) = v_2(t) \\ \dot{v}_2(t) = R^2 \begin{cases} -\ell_1 arsh\left[\lambda_1 \left(v_1(t) - \alpha(t)\right)\right] \\ -\ell_2 arsh\left(\lambda_2 v_2(t)/R\right) \end{cases} \end{cases} \tag{9}$$

where $\alpha(t)$ is the input signal. $v_1(t), v_2(t)$ are the state variables of tracking differentiator. $R, \ell_1, \ell_2, \lambda_1, \lambda_2$ are the positive constants. With properly design constants $R, \ell_1, \ell_2, \lambda_1, \lambda_2$ and R is big enough, when the input signal α passes through the differentiator (9), the following theorem holds

Lemma 1 [30]: For the following system

$$\begin{cases} \dot{v}_1(t) = v_2(t) \\ \dot{v}_2(t) = R^2 g\left[\left(v_1(t) - \alpha(t)\right), v_2(t)/R\right] \end{cases} \tag{10}$$

The solution of system (10) satisfies

$$\lim_{R\to\infty} \int_0^T \left|v_1(t) - \alpha(t)\right| dt = 0 \tag{11}$$

where $g(\cdot)$ denotes a smooth bounded function. $R > 0$ represents a design constant. $\alpha(t)$ is a bounded integrable function. Lemma 1 ensures that when R is large enough, the solution $v_1(t)$ of equation (10) can fully approximate the input signal $\alpha(t)$ in arbitrary finite time, thus the following formula holds

$$\dot{v}_1(t) = v_2(t) = \dot{\alpha}(t) \tag{12}$$

Lemma 2 [31]: If the condition $v_1(t) - \alpha(t) \le \kappa$ with $\kappa > 0$, then it has positive constant l_{v2} which satisfies the following inequality

$$\left|v_2(t) - \dot{\alpha}(t)\right| \le l_{v2} \tag{13}$$

Assumption 2: For facilitating controller design and avoiding the explosion of complexity. Assuming that $x_{1d} = \alpha_1$, so $\dot{\alpha}_i, i = 1, 2, 3, 4$ can be written by letting pass through the IHSFTD as:

$$\begin{cases} \dot{v}_{i1} = v_{i2} \\ \dot{v}_{i2} = R_i^2 \left\{-\ell_{i1} arsh\left[\lambda_{i1}(v_{i1} - \alpha_i)\right]\right. \\ \left. -\ell_{i2} arsh\left(\lambda_{i2} v_{i2}/R_i\right)\right\} \end{cases} \tag{14}$$

where $|v_{i2} - \dot{\alpha}_i| \le l_{vi2}$, and $R_i, \ell_{i1}, \ell_{i2}, \lambda_{i1}, \lambda_{i2}, l_{vi2}$ are the positive design constants

C. CHEBYSHEV NEURAL NETWORK

The Chebyshev polynomial can be obtained from the following second order recursive equation [25]

$$T_{i+1}(X) = 2XT_i(X) - T_{i-1}(X), \quad T_0(X) = 1 \tag{15}$$

where $X \in \mathbb{R}$, $T_1(X)$ is usually expressed as $X, 2X, 2X-1$ or $2X+1$.

The Chebyshev neural network is capable of approximating any nonlinear continuous function $F^*(x)$ over a compact set to any degree of accuracy. A strengthened pattern about the Chebyshev multinomial for $X = [x_1, \ldots, x_m]^T \in \mathbb{R}^m$ is presented as

$$\zeta(X) = \begin{bmatrix} 1, T_1(x_1), \ldots, T_n(x_1), \ldots, \\ T_1(x_m), \ldots, T_n(x_m) \end{bmatrix} \tag{16}$$

where $T_i(x_j), i = 1, \ldots, n, j = 1, \ldots, m, n$ stands for the order, m denotes the Chebyshev multinomial, $\zeta(x)$ represents the Chebyshev multinomial basis function vector.

According to the above descriptions, the arbitrary unknown nonlinear function can be formulated as

$$F(X) = W^{*T}\zeta(X) + \delta \tag{17}$$

where W^* denotes the desired weight vector, δ is the approximation error, and there exists known constants δ_0, which satisfies $0 < |\delta| < \delta_0$.

W^* can be defined as

$$W^* = \arg\min_{W\in\Omega_W} \left\{ \sup_{X\in D_x} \left|F(X) - \hat{W}^T\zeta(X)\right| \right\} \tag{18}$$

where Ω_W and D_X are the compact set of reasonable bounds of W and X, respectively.

Assumption 3: There is a positive constant δ_M which satisfies $|\delta_i| \le \delta_M, i = 1, 2$.

D. TANGENT BARRIER FUNCTION

For the sake of ensuring that system state is bounded in a desired region, a tangent barrier function $y\tan(y)$ is employed in this paper, where $\tan(\cdot)$ stands for the tangent function. It is obvious that the tangent barrier function satisfies the characteristics listed as below:

$$+\infty > y\tan(y) \ge 0 \text{ for } y \in (-\pi/2, \pi/2) \tag{19}$$

According to the above descriptions, we can formalize the results for general forms of tangent barrier function in Lyapunov synthesis satisfying $y\tan(y) \to \infty$ as $y \to -\pi/2$ or $y \to \pi/2$.

III. ADAPTIVE CONTROL BASED ON BACKSTEPPING

A. CONTROLLER DESIGN

According to the above-mentioned dynamics system, the whole design process consists of four phases. Then, the controller design process is described in detail.

Step 1: Choosing the first Lyapunov function as

$$V_1 = e_1 \tan\left(\frac{\pi}{2r_1}e_1\right) \tag{20}$$

where the design parameter $r_1 = a - d > 0\,(a > d)$ denotes the constraint on e_1. That is, $e_1 \in (-r_1, r_1)$.

With (20), the time derivative of V_1 is expressed as:

$$\begin{aligned} \dot{V}_1 &= \dot{e}_1 \left[\tan\left(\frac{\pi}{2r_1}e_1\right) + \frac{\pi}{2r_1}e_1 \sec^2\left(\frac{\pi}{2r_1}e_1\right)\right] \\ &= (x_2 - \dot{x}_{1d})M \end{aligned} \tag{21}$$

where $M = \tan\left(\frac{\pi}{2r_1}e_1\right) + \frac{\pi}{2r_1}e_1 \sec^2\left(\frac{\pi}{2r_1}e_1\right)$

Then, according to (21), the virtual control input α_2 is defined by the following equality:

$$\alpha_2 = -k_1 M + v_{12} \tag{22}$$

where $k_1 > 0$ is the design constant.

Substituting (22) into (23), one has

$$\dot{V}_1 \leq -\left(k_1 - \frac{1}{2}\right) M^2 + e_2 M + \frac{1}{2} l_{v12}^2 \tag{23}$$

Step 2: Choosing the second Lyapunov function as

$$V_2 = V_1 + \frac{1}{2} J_l e_2^2 + \frac{1}{2\Gamma_1} \tilde{\vartheta}_1^2 + \frac{1}{2} \omega \tilde{z}^2 + \frac{1}{2\eta_1} \tilde{\omega}^2 + \frac{1}{2\eta_2} \tilde{\upsilon}^2 \tag{24}$$

where $\Gamma_1 > 0, \eta_1 > 0, \eta_2 > 0$ are designed control parameters, $\tilde{\omega} = \hat{\omega} - \omega$, $\tilde{\upsilon} = \hat{\upsilon} - \upsilon$, $\tilde{\vartheta}_1 = \hat{\vartheta}_1 - \vartheta_1$, and $\hat{\omega}, \hat{\upsilon}, \hat{\vartheta}_1$ denote the estimate value of $\omega, \upsilon, \vartheta_1$.

With (24), the time derivative of V_2 is expressed as the following inequation:

$$\begin{aligned} \dot{V}_2 \leq & -\left(k_1 - \frac{1}{2}\right) M^2 + e_2 M + \frac{1}{2} l_{v12}^2 \\ & + J_l e_2 \left\{ \frac{1}{J_l} \left[-c_1 x_2 - F_f - d_l + K \left(\frac{x_3}{N} - x_1 \right) \right] - \dot{\alpha}_2 \right\} \\ & + \frac{1}{\Gamma_1} \tilde{\vartheta}_1 \dot{\hat{\vartheta}}_1 + \omega \tilde{z} \left(\dot{\hat{z}} - \dot{z} \right) + \frac{1}{\eta_1} \tilde{\omega} \dot{\hat{\omega}} + \frac{1}{\eta_2} \tilde{\upsilon} \dot{\hat{\upsilon}} \end{aligned} \tag{25}$$

By using the Chebyshev neural network to approximate the unknown external disturbance d_l, it can be obtained that

$$d_l = \theta_1^T \xi_1 + \delta_1 \tag{26}$$

where δ_1 is the approximation error and satisfies $|\delta_1| \leq \delta_M$.

By utilizing the Young's inequality, one can obtain

$$\begin{aligned} e_2 d_l &= e_2 \left(\theta_1^T \xi_1 + \delta_1 \right) \\ &\leq \frac{1}{2m_1^2} e_2^2 \vartheta_1 \xi_1^T \xi_1 + \frac{1}{2} m_1^2 + \frac{1}{2} e_2^2 + \frac{1}{2} \delta_{10}^2 \end{aligned} \tag{27}$$

where $\vartheta_1 = \|W_1\|^2 = W_1^T W_1$, which can reduce the numbers of weights for the Chebyshev neural network, ϑ_1 and $\|\cdot\|$ are the unknown variable and the 2-norms of W_1, respectively, and m_1 is the design constant.

Substituting (27) into (25) yields

$$\begin{aligned} \dot{V}_2 \leq & e_2 \begin{bmatrix} -c_1 x_2 - F_f + K \left(\frac{x_3}{N} - x_1 \right) + M \\ + \frac{1}{2m^2} \vartheta_1 e_2 \xi_1^T \xi_1 + \frac{1}{2} e_2 - J_l \dot{\alpha}_2 \end{bmatrix} \\ & - \left(k_1 - \frac{1}{2}\right) M^2 + \frac{1}{2} l_{v12}^2 + \frac{1}{\Gamma_1} \tilde{\vartheta}_1 \dot{\hat{\vartheta}}_1 + \frac{1}{2} m_1^2 + \frac{1}{2} \delta_{10}^2 \\ & + \omega \tilde{z} \left(\dot{\hat{z}} - \dot{z} \right) + \frac{1}{\eta_1} \tilde{\omega} \dot{\hat{\omega}} + \frac{1}{\eta_2} \tilde{\upsilon} \dot{\hat{\upsilon}} \end{aligned} \tag{28}$$

Since the average deflection of bristles cannot be measured directly, a nonlinear state observer is used to estimate z, one has

$$\dot{\hat{z}} = x_2 - \frac{|x_2|}{g(x_2)} \hat{z} - \left(\sigma_0 - \sigma_1 \frac{|x_2|}{g(x_2)} \right) e_2 \tag{29}$$

where $\hat{z}$ is the estimated value of z, and $\tilde{z} = \hat{z} - z$ is the estimation error of z.

The estimated value of friction torque is:

$$\hat{F}_f = \hat{\omega} \left(\sigma_0 \hat{z} + \sigma_1 \dot{\hat{z}} \right) + \hat{\upsilon} \sigma_2 x_2 \tag{30}$$

where $\hat{F}_f$ is the estimated value of F_f.

Then, the virtual control input α_3 and adaptive law $\dot{\hat{\vartheta}}_1, \dot{\hat{\omega}}, \dot{\hat{\upsilon}}$ are given as follows

$$\alpha_3 = \frac{N}{K} \begin{pmatrix} c_1 x_2 + \hat{F}_f + K x_1 - M \\ -\frac{1}{2m_1^2} \hat{\vartheta}_1 e_2 \xi_1^T \xi_1 - \frac{1}{2} e_2 - k_2 e_2 + J_l v_{22} \end{pmatrix} \tag{31}$$

$$\dot{\hat{\vartheta}}_1 = \frac{1}{2m_1^2} \Gamma_1 e_2^2 \xi_1^T \xi_1 - c_1 \hat{\vartheta}_1 \tag{32}$$

$$\dot{\hat{\omega}} = -\eta_1 e_2 \begin{bmatrix} \left(\sigma_0 - \sigma_1 \frac{|x_2|}{g(x_2)} \right) \hat{z} + \sigma_1 x_2 \\ -\sigma_1 \left(\sigma_0 - \sigma_1 \frac{|x_2|}{g(x_2)} \right) e_2 \end{bmatrix} \tag{33}$$

$$\dot{\hat{\xi}} = -\eta_2 e_2 \sigma_2 x_2 \tag{34}$$

where $k_2 > 0$ and $c_1 > 0$ are the design constants.

Noting that $-\frac{c_1}{\Gamma_1} \hat{\vartheta}_1 \tilde{\vartheta}_1 \leq -\frac{c_1}{2\Gamma_1} \left| \tilde{\vartheta}_1 \right|^2 + \frac{c_1}{2\Gamma_1} |\vartheta_1|^2$, using Young's inequality and combining equations (28), (31), (32), (33) and (34), we obtain

$$\begin{aligned} \dot{V}_2 \leq & -\left(k_1 - \frac{1}{2}\right) M^2 - \left(k_2 - \frac{1}{2}\right) e_2^2 + \frac{K}{N} e_2 e_3 + \frac{1}{2} \delta_{10}^2 \\ & + \frac{1}{2} m_1^2 - \frac{c_1}{2\Gamma_1} \left| \tilde{\vartheta}_1 \right|^2 + \frac{c_1}{2\Gamma_1} |\vartheta_1|^2 \\ & + \frac{1}{2} l_{v12}^2 + \frac{1}{2} J_l^2 l_{v22}^2 - \omega h \tilde{z}^2 \end{aligned} \tag{35}$$

where $h = |x_2| / g(x_2)$ is bounded.

Step 3: Choosing the third Lyapunov function as

$$V_3 = V_2 + \frac{1}{2} e_3^2 \tag{36}$$

Computing the derivative of V_3, it gives

$$\begin{aligned} \dot{V}_3 \leq & e_3 (x_4 - \dot{\alpha}_3) - \left(k_1 - \frac{1}{2}\right) M^2 - \left(k_2 - \frac{1}{2}\right) e_2^2 \\ & + \frac{K}{N} e_2 e_3 + \frac{1}{2} \delta_{10}^2 + \frac{1}{2} m_1^2 - \frac{c_1}{2\Gamma_1} \left| \tilde{\vartheta}_1 \right|^2 + \frac{c_1}{2\Gamma_1} |\vartheta_1|^2 \\ & + \frac{1}{2} l_{v12}^2 + \frac{1}{2} J_l^2 l_{v22}^2 - \varphi h \tilde{z}^2 \end{aligned} \tag{37}$$

Then, defining the virtual control α_4 as

$$\alpha_4 = -k_3 e_3 - \frac{K}{N} e_2 + v_{32} \tag{38}$$

where $k_3 > 0$ is the design constant.

Substituting (38) into (37), one has

$$\begin{aligned} \dot{V}_3 \leq & -\left(k_1 - \frac{1}{2}\right) M^2 - \left(k_2 - \frac{1}{2}\right) e_2^2 - \left(k_3 - \frac{1}{2}\right) e_3^2 \\ & + e_3 e_4 + \frac{1}{2} \delta_{10}^2 + \frac{1}{2} m_1^2 - \frac{c_1}{2\Gamma_1} \left| \tilde{\vartheta}_1 \right|^2 + \frac{c_1}{2\Gamma_1} |\vartheta_1|^2 \\ & + \frac{1}{2} l_{v12}^2 + \frac{1}{2} J_l^2 l_{v22}^2 + \frac{1}{2} l_{v32}^2 - \varphi h \tilde{z}^2 \end{aligned} \tag{39}$$

Step 4: Choosing the fourth Lyapunov function as

$$V_4 = V_3 + \frac{1}{2}J_m e_4^2 + \frac{1}{2\Gamma_2}\tilde{\vartheta}_2^2 \tag{40}$$

where $\Gamma_2 > 0$, and the definition $\tilde{\vartheta}_2 = \hat{\vartheta}_2 - \vartheta_2$ is similar to that of $\tilde{\vartheta}_1$.

Next, the time derivative of V_4 is calculated as

$$\begin{aligned}\dot{V}_4 \le\ & e_4\left[u - c_2x_4 - \frac{K}{N}\left(\frac{x_3}{N} - x_1\right) - d_m - J_m\dot{\alpha}_4\right] \\ & - \left(k_1 - \frac{1}{2}\right)M^2 - \left(k_2 - \frac{1}{2}\right)e_2^2 - \left(k_3 - \frac{1}{2}\right)e_3^2 + e_3e_4 \\ & + \frac{1}{\Gamma_2}\tilde{\vartheta}_2\dot{\hat{\vartheta}}_2 + \frac{1}{2}\delta_{10}^2 + \frac{1}{2}m_1^2 - \frac{c_1}{2\Gamma_1}\left|\tilde{\vartheta}_1\right|^2 + \frac{c_1}{2\Gamma_1}|\vartheta_1|^2 \\ & + \frac{1}{2}l_{v12}^2 + \frac{1}{2}J_l^2 l_{v22}^2 + \frac{1}{2}l_{v32}^2 - \varphi h\tilde{z}^2\end{aligned} \tag{41}$$

By using the Chebyshev neural network to approximate the unknown external disturbance d_m, it can be obtained that

$$d_m = \theta_2^T\xi_2 + \delta_2 \tag{42}$$

where δ_2 is the approximation error and satisfies $|\delta_2| \le \delta_M$.

Similarly, utilizing the Young's inequality, it obtains

$$\begin{aligned}e_4d_m &= e_4\left(\theta_2^T\xi_2 + \delta_2\right) \\ &\le \frac{1}{2m_2^2}e_4^2\vartheta_2\xi_2^T\xi_2 + \frac{1}{2}m_2^2 + \frac{1}{2}e_4^2 + \frac{1}{2}\delta_{20}^2\end{aligned} \tag{43}$$

where $m_2 > 0$ is the design constant and $\hat{\vartheta}_2 = \left\|\hat{W}_2\right\|^2$.

Substituting (43) into (41), one has

$$\begin{aligned}\dot{V}_4 \le\ & e_4\left[\begin{array}{l}u - c_2x_4 - \frac{K}{N}\left(\frac{x_3}{N} - x_1\right) \\ + \frac{1}{2m_2^2}e_4\vartheta_2\xi_2^T\xi_2 + e_3 + \frac{1}{2}e_4 - J_m\dot{\alpha}_4\end{array}\right] \\ & - \left(k_1 - \frac{1}{2}\right)M^2 - \left(k_2 - \frac{1}{2}\right)e_2^2 - \left(k_3 - \frac{1}{2}\right)e_3^2 \\ & + \frac{1}{\Gamma_2}\tilde{\vartheta}_2\dot{\hat{\vartheta}}_2 + \sum_{i=1}^{2}\frac{1}{2}\delta_{i0}^2 + \sum_{i=1}^{2}\frac{1}{2}m_i^2 - \frac{c_1}{2\Gamma_1}\left|\tilde{\vartheta}_1\right|^2 \\ & + \frac{c_1}{2\Gamma_1}|\vartheta_1|^2 + \frac{1}{2}l_{v12}^2 + \frac{1}{2}J_l^2 l_{v22}^2 + \frac{1}{2}l_{v32}^2 - \varphi h\tilde{z}^2\end{aligned} \tag{44}$$

Then, the control input u with adaptive law $\dot{\hat{\vartheta}}_2$ is designed as

$$\begin{aligned}u = & c_2x_4 + \frac{K}{N}\left(\frac{x_3}{N} - x_1\right) - \frac{1}{2m_2^2}e_4\hat{\vartheta}_2\xi_2^T\xi_2 \\ & - e_3 - \frac{1}{2}e_4 + J_m v_{42} - k_4e_4\end{aligned} \tag{45}$$

$$\dot{\hat{\vartheta}}_2 = \frac{1}{2m_2^2}\Gamma_2 e_4^2\xi_2^T\xi_2 - c_2\hat{\vartheta}_2 \tag{46}$$

where $k_4 > 0$ and $c_2 > 0$ are the design constants.

Noting that $-\frac{c_2}{\Gamma_2}\hat{\vartheta}_2\tilde{\vartheta}_2 \le -\frac{c_2}{2\Gamma_2}\left|\tilde{\vartheta}_2\right| + \frac{c_2}{2\Gamma_2}|\vartheta_2|^2$ and using Young's inequality, equation (45) can be simplified as

$$\begin{aligned}\dot{V}_4 \le & -\left(k_1 - \frac{1}{2}\right)M^2 - \left(k_2 - \frac{1}{2}\right)e_2^2 - \left(k_3 - \frac{1}{2}\right)e_3^2 \\ & - \left(k_4 - \frac{1}{2}\right)e_4^2 - \frac{c_1}{2\Gamma_1}\left|\tilde{\vartheta}_1\right|^2 + \frac{c_1}{2\Gamma_1}|\vartheta_1|^2 - \frac{c_2}{2\Gamma_2}\left|\tilde{\vartheta}_2\right|^2 \\ & + \frac{c_2}{2\Gamma_2}|\vartheta_2|^2 + \sum_{i=1}^{2}\frac{1}{2}\delta_{i0}^2 + \sum_{i=1}^{2}\frac{1}{2}m_i^2 + \frac{1}{2}l_{v12}^2 + \frac{1}{2}J_l^2 l_{v22}^2 \\ & + \frac{1}{2}l_{v32}^2 + \frac{1}{2}J_m^2 l_{v42}^2 - \varphi h\tilde{z}^2\end{aligned} \tag{47}$$

B. STABILITY ANALYSIS

For any given constant p, the closed sets can be defined as

$$\left\{\begin{array}{l}\Pi_1 = \{(e_1) : 2V_1 \le 2p\} \\ \Pi_2 = \left\{\left(e_1, e_2, \hat{\vartheta}_1\right) : 2V_1 + e_2^2 + \frac{1}{\Gamma_1}\tilde{\vartheta}_1^2 \le 2p\right\} \\ \Pi_3 = \left\{\begin{array}{l}\left(e_1, e_2, e_3, \hat{\vartheta}_1\right) : \\ 2V_1 + \sum_{i=2}^{3}e_i^2 + \frac{1}{\Gamma_1}\tilde{\vartheta}_1^2 \le 2p\end{array}\right\} \\ \Pi_4 = \left\{\begin{array}{l}\left(e_1, e_2, e_3, e_4, \hat{\vartheta}_1, \hat{\vartheta}_2\right) : \\ 2V_1 + \sum_{i=2}^{4}e_i^2 + \sum_{i=1}^{2}\frac{1}{\Gamma_i}\tilde{\vartheta}_i^2 \le 2p\end{array}\right\}\end{array}\right. \tag{48}$$

Theorem 1: For the HD system (7) subject to output constrained under Lemmas 1-3 and Assumptions 1-3, the controller (45) and the adaptive laws (32), (33), (34), (46) are obtained. If initial conditions satisfy Π_i, $r_1(0) \in (-r_{10}, r_{10})$, where $i = 1, 2, 3, 4$, Then the raised control scheme can guarantee that all the objectives are realized.

Proof: The differentiation of the Lyapunov function candidate in relation to t is derived as

$$\begin{aligned}\dot{V} = & -\left(k_1 - \frac{1}{2}\right)M^2 - \left(k_2 - \frac{1}{2}\right)e_2^2 - \left(k_3 - \frac{1}{2}\right)e_3^2 \\ & - \left(k_4 - \frac{1}{2}\right)e_4^2 - \sum_{i=1}^{2}\frac{c_i}{2\Gamma_i}\left|\tilde{\vartheta}_i\right|^2 - \varphi h\tilde{z}^2 + \Xi\end{aligned} \tag{49}$$

Namely

$$\dot{V} \le -\beta V + \Xi \tag{50}$$

where

$$\beta = \min\left\{\begin{array}{l}2\left(k_1 - \frac{1}{2}\right), 2\left(k_2 - \frac{1}{2}\right), 2\left(k_3 - \frac{1}{2}\right), \\ 2\left(k_4 - \frac{1}{2}\right), c_1, c_2, 2H\end{array}\right\} > 0 \text{ and}$$

$$\begin{aligned}\Xi = & \sum_{i=1}^{2}\frac{c_i}{2\Gamma_i}|\vartheta_i|^2 + \sum_{i=1}^{2}\frac{1}{2}\delta_{i0}^2 + \sum_{i=1}^{2}\frac{1}{2}m_i^2 \\ & + \frac{1}{2}l_{v12}^2 + \frac{1}{2}J_l^2 l_{v22}^2 + \frac{1}{2}l_{v32}^2 + \frac{1}{2}J_m^2 l_{v42}^2\end{aligned}$$

Let $\beta > \Xi/p$, when $V = p$, it has $\dot{V} \leq 0$, therefore, $V \leq p$ is an invariant set. That is $\forall t \geq 0$, if $V(0) \leq p$, it has $V(t) \leq p$.

Solving equation (50) yields:

$$0 \leq V(t) \leq \frac{\Xi}{\beta} + \left(V(0) - \frac{\Xi}{\beta}\right) e^{-\beta t} \tag{51}$$

Equation (51) indicates that $V(t)$ is ultimately bounded by $\beta > \Xi/p$. Therefore, all errors $\left(e_i, \tilde{\vartheta}_j, \tilde{z}\right), j = 1, 2$ in the closed-loop system are ultimately uniformly bounded. In addition, by adjusting the value of $k_i, \Gamma_j, m_j, c_j, R_i, l_{ij}, \lambda_{ij}$, the value of Ξ/p can be arbitrarily small. Therefore, the position tracking error e_1 can be arbitrarily small.

Remark 1: The larger k_i and Γ_j can obtain good tracking performance. But too k_i and Γ_j can result in large control input, which may be far beyond physical limitations of HD systems. Meanwhile, the large R_i and small l_{ij}, λ_{ij} can improve the accuracy of tracking differentiator. However, too large R_i can make tracking position have obvious step oscillation at the beginning. Besides, the relatively large m_j and small c_j can improve the approximation performance of neural network.

IV. SIMULATIONS ANALYSIS

In this section, we validate the stable tracking behavior through numerical simulation to confirm the effectiveness and robustness of the proposed scheme. Additionally, we evaluate the tracking performance by comparing three aspects: the maximum (MAX), the average (AVG), and the standard deviation (SD) indexes. The nominal dynamic parameters of the HD system are presented in Table 1, while the parameters of the LuGre friction model can be found in Table 2. Next, we describe the main design parameters as follows: $r_1 = 0.02, k_1 = 20, k_2 = k_3 = k_4 = 50, m_1 = m_2 = 100, c_1 = c_2 = 0.01R_1 = 20, R_2 = R_3 = R_4 = 30, \ell_{12} = \ell_{13} = \ell_{14} = 2, \ell_{11} = 1, \ell_{21} = 1, \lambda_{11} = 1, \ell_{22} = \ell_{23} = \ell_{24} = 1.5, \lambda_{12} = \lambda_{13} = \lambda_{14} = 2, \lambda_{21} = 1, \lambda_{22} = \lambda_{23} = \lambda_{24} = 1.5$.

In addition, the Chebyshev basis functions are selected by

$$\zeta_i = \begin{cases} \left[1, x_1, 2x_1^2 - 1, 4x_1^3 - 3x_1, x_2, 2x_2^2 - 1, 4x_2^3 - 3x_2\right]^T \\ \left[1, x_3, 2x_3^2 - 1, 4x_3^3 - 3x_3, x_4, 2x_4^2 - 1, 4x_4^3 - 3x_4\right]^T \end{cases}, \quad i = 1, 2,$$

The external disturbances are applied at the load and motor ends as follow $d_l = \begin{cases} 0 & (t < 2) \\ 50 & (t \geq 2) \end{cases}, d_m = \begin{cases} 0 & (t < 2) \\ 10 & (t \geq 2) \end{cases}$. The initial value of the state variables of the system are all set as $\bar{x}_0 = [0, 0, 0, 0]$, and the reference trajectory is defined as $x_{1d} = 1 - \cos(t)$.

Figs. 1(a)-(b) illustrate the comparison of tracking effects between ANBC and RBFDSC on reference trajectories under output constraints, with fixed LuGre friction parameters. As shown in Fig. 1(a), both ANBC and RBFDSC can accurately track the reference trajectory. However, upon closer inspection in the magnified image, it is apparent that the trajectory of ANBC closely aligns with the reference trajectory. This observation is further supported by the error data presented in Table 3 and Fig. 2(b). The MAX, AVG, and SD of the tracking errors obtained using the proposed ANBC are smaller than those achieved with RBFDSC. Additionally, it is worth noting that the tracking error of ANBC remains within the predefined region bounds, unlike that of RBFDSC. Consequently, we can deduce that when output is constrained, ANBC can enhance the tracking performance of a given signal.

Figs. 2(a)-(b) illustrate the compensation of the neural network for the external unknown disturbance torques at both the load and motor ends. As observed in Figs. 2(a)-(b), T2SFNN1 and T2SFNN2 exhibit a swift response, accurately tracking the desired trajectory with minimal error, even after the application of an external disturbance torque.

TABLE 1. HD system model parameters.

Symbol	Denotation	Value
J_l	moment of inertia at the load end	1.5×10^{-3}kg·m^2
J_m	moment of inertia at the motor end	4.8×10^{-3}kg·m^2
K	stiffness coefficient	200Nm·rad^{-1}
N	reduction ratio	80
C_l	damping coefficient at the load end	0.01Nm·rad^{-1}
C_2	damping coefficient at the motor end	0.01Nm·rad^{-1}
d_l	unknown disturbance torque at the load end	50Nm
d_m	unknown disturbance torque at the motor end	10Nm

TABLE 2. LuGre friction model parameters.

Symbol	Denotation	Value
σ_0	stiffness coefficient	259Nm·rad^{-1}
σ_1	damping coefficient	7Nm·rad^{-1}
σ_2	viscous friction coefficient	4.93Nm·rad^{-1}
F_c	coulomb friction	9.42Nm
F_s	stiction force	7.97Nm
q_s	stribeck angular speed	0.04rad·s

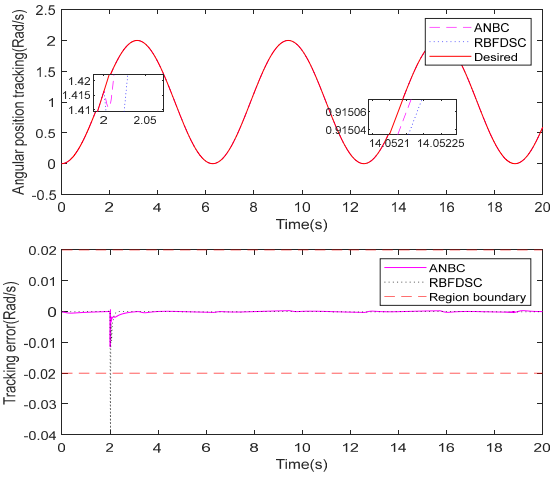

FIGURE 1. Trajectory tracking results with fixed LuGre friction parameters. (a) Angular position tracking curve. (b) Tracking error curve.

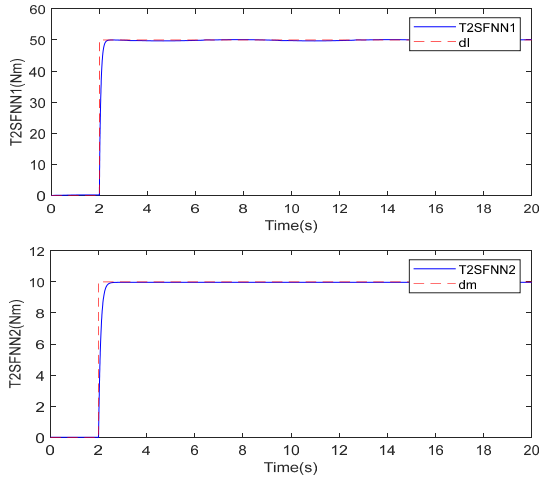

FIGURE 2. Approximation of T2SFNN to unknown external disturbances. (a) Approximation to dl at the load end (b) Approximation to dm at the motor end.

TABLE 3. Comparisons of angular tracking errors e_1 with fixed LuGre friction parameters.

Controller	ANBC	RBFDSC
MAX(rad)	0.0116	0.0385
AVG(rad)	0.0002	0.0003
SD(rad)	0.0008	0.0026

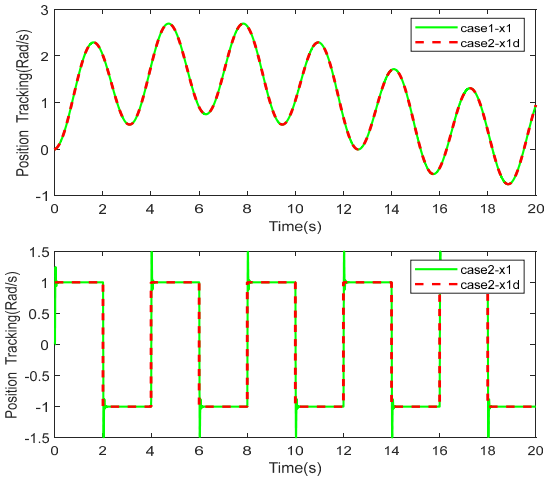

FIGURE 3. Trajectory tracking results with two different reference trajectory.

To verify the dynamic performance of the proposed ANBC. We reset the reference trajectory as follows:

Case 1: x_{1d} is reset as a mix frequency sinusoidal function $x_{1d} = 1 - \cos(2t) + 0.75\sin(0.25t)$.

Case 2: x_{1d} is reset to a square wave function with Amplitude =1 and Frequency =0.25.

Fig. 3 shows that the ANBC can still achieve effective tracking when the reference trajectory is set as the mix frequency sinusoidal function or a square wave function.

To further validate the robustness of the proposed adaptive control algorithm, we analyzed the tracking performance on

TABLE 4. LuGre friction model dynamic parameters.

Symbol	Denotation	Value
σ_0	stiffness coefficient	259×[1+0.2sin(0.2t)]Nm·rad^{-1}
σ_1	damping coefficient	7×[1+0.3sin(0.2t)]Nm·rad^{-1}
σ_2	viscous friction coefficient	4.93×[1+0.4sin(0.2t)]Nm·rad^{-1}
F_c	coulomb friction	9.42×[1+0.3sin(0.2t)]Nm
F_s	stiction force	7.97×[1+0.2sin(0.2t)]Nm
q_s	stribeck angular speed	0.04×[1+0.5sin(0.2t)]rad·s

TABLE 5. Comparisons of angular tracking errors e_1 with dynamic LuGre friction parameters.

Controller	ANBC	RBFDSC
MAX(rad)	0.0120	0.0505
AVG(rad)	0.0004	0.0010
SD(rad)	0.0009	0.0048

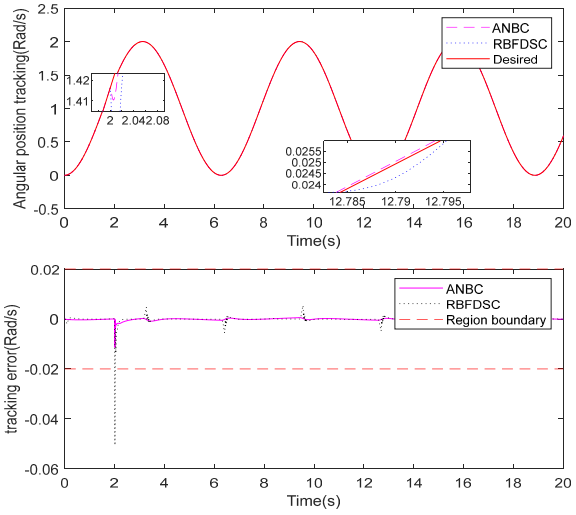

FIGURE 4. Trajectory tracking results with dynamic LuGre friction parameters. (a) Angular position tracking curve. (b) Tracking error curve.

the LuGre model with dynamic parameters. The dynamic changes in the LuGre friction model parameters were selected and are listed in Table 4.

Figs. 4(a)-(b) demonstrate the position tracking and tracking errors of the two controllers when the parameters of the LuGre friction model dynamically change. Observing these figures, it is evident that the RBFDSC controller deviates noticeably from the desired trajectory, while the ANBC controller effectively tracks the desired signal. Additionally, the tracking error of ANBC remains within the predefined region bounds. Moreover, as indicated in Table 5, the ANBC controller outperforms the RBFDSC controller in terms of MAX, AVG, and SD of the tracking error in the same scenario.

Figs. 5(a)-(b) showcase the friction compensation effects and friction compensation errors of the two controllers under dynamic parameter changes in the LuGre model. It is observed that when the parameters of the LuGre model change dynamically, the proposed modified adaptive method accurately compensates for the actual friction force, while the RBFDSC method, without modified parameters, exhibits more pronounced deviations in friction compensation.

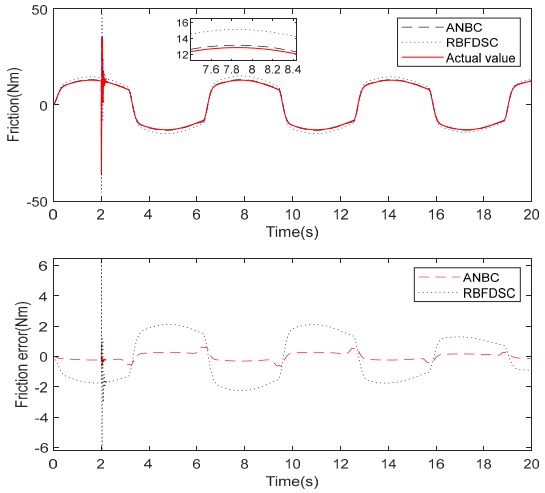

FIGURE 5. Friction compensation of Lugre model with dynamic parameters. (a) Friction compensation curve. (b) Friction compensation error curve.

In summary, the simulation results confirm that the proposed ANBC controller effectively tracks the desired signal in the presence of disturbances, output constraints, and dynamic LuGre friction parameters. Furthermore, the comparative analysis between ANBC and RBFDSC demonstrates that ANBC achieves higher precision tracking performance for the harmonic drive system. These findings support the conclusion that the adaptive controller proposed in this paper enables accurate control and exhibits robustness.

V. CONCLUSION

To address the challenges of nonlinear friction and external disturbances in the HD system, an ANBC scheme with friction compensation, incorporating a modified LuGre model, has been developed. This scheme aims to reduce the effect of nonlinear friction by introducing average mane deformation and viscous friction coefficients. Additionally, a Chebyshev neural network is integrated into the control strategy to enhance robustness against external disturbances at both the load and motor ends. Simultaneously, the TBLF ensures that the tracking error approximates the desired signal within a small margin, while adhering to certain restrictions. Stability analysis of the closed-loop HD system is conducted using the Lyapunov criterion. Simulation results demonstrate that the proposed ANBC method exhibits greater robustness compared to RBFDSC against changes in friction parameters and external disturbances, leading to enhanced position-tracking accuracy in the HD system.

Future research will focus on designing adaptive controllers that utilize neural network approximations for friction compensation while considering the impact of factors such as hysteresis and nonlinear stiffness on the HD system.

REFERENCES

[1] J. Wang, Z. Wan, Z. Dong, and Z. Li, "Research on performance test system of space harmonic reducer in high vacuum and low temperature environment," *Machines*, vol. 9, no. 1, p. 1, Dec. 2020.

[2] Y. He, J. Chen, X. Zhou, and S. Huang, "In-situ fault diagnosis for the harmonic reducer of industrial robots via multi-scale mixed convolutional neural networks," *J. Manuf. Syst.*, vol. 66, pp. 233–247, Feb. 2023.

[3] B. Han, J. Ma, and H. Li, "Research on nonlinear friction compensation of harmonic drive in gimbal servo-system of DGCMG," *Int. J. Control, Autom. Syst.*, vol. 14, no. 3, pp. 779–786, Jun. 2016.

[4] Z.-C. Qiu, J.-D. Han, and J.-G. Liu, "Experiments on fuzzy sliding mode variable structure control for vibration suppression of a rotating flexible beam," *J. Vibrat. Control*, vol. 21, no. 2, pp. 343–358, Feb. 2015.

[5] H. Yu, H. Gao, H. Deng, S. Yuan, and L. Zhang, "Synchronization control with adaptive friction compensation of treadmill-based testing apparatus for wheeled planetary rover," *IEEE Trans. Ind. Electron.*, vol. 69, no. 1, pp. 592–603, Jan. 2022.

[6] P. Chen, X. Liu, and Q. Yan, "Adaptive friction compensation for a class of mechanical systems based on LuGre model," *Int. J. Robust Nonlinear Control*, vol. 32, no. 7, pp. 4510–4534, May 2022.

[7] W. Zhang, M. Li, Y. Gao, and Y. Chen, "Periodic adaptive learning control of PMSM servo system with LuGre model-based friction compensation," *Mechanism Mach. Theory*, vol. 167, Jan. 2022, Art. no. 104561.

[8] P. Tomei, "Robust adaptive friction compensation for tracking control of robot manipulators," *IEEE Trans. Autom. Control*, vol. 45, no. 11, pp. 2164–2169, Nov. 2000.

[9] H. M. Kim, S. H. Park, and S. I. Han, "Precise friction control for the nonlinear friction system using the friction state observer and sliding mode control with recurrent fuzzy neural networks," *Mechatronics*, vol. 19, no. 6, pp. 805–815, Sep. 2009.

[10] F. Yue and X. Li, "Adaptive sliding mode control based on friction compensation for opto-electronic tracking system using neural network approximations," *Nonlinear Dyn.*, vol. 96, no. 4, pp. 2601–2612, Jun. 2019.

[11] X. Zhou, B. Zhao, W. Liu, H. Yue, R. Yu, and Y. Zhao, "A compound scheme on parameters identification and adaptive compensation of nonlinear friction disturbance for the aerial inertially stabilized platform," *ISA Trans.*, vol. 67, pp. 293–305, Mar. 2017.

[12] L. Lu, B. Yao, Q. Wang, and Z. Chen, "Adaptive robust control of linear motors with dynamic friction compensation using modified LuGre model," *Automatica*, vol. 45, no. 12, pp. 2890–2896, Dec. 2009.

[13] K. Dai, Z. Zhu, G. Shen, Y. Tang, X. Li, W. Wang, and Q. Wang, "Adaptive force tracking control of electrohydraulic systems with low load using the modified LuGre friction model," *Control Eng. Pract.*, vol. 125, Aug. 2022, Art. no. 105213.

[14] J. Yao, W. Deng, and Z. Jiao, "Adaptive control of hydraulic actuators with LuGre model-based friction compensation," *IEEE Trans. Ind. Electron.*, vol. 62, no. 10, pp. 6469–6477, Oct. 2015.

[15] F. Yue and X. Li, "Robust adaptive integral backstepping control for opto-electronic tracking system based on modified LuGre friction model," *ISA Trans.*, vol. 80, pp. 312–321, Sep. 2018.

[16] P. Soleimanian and H. Ahmadian, "Modeling friction effects in lubricated roller guideways using a modified LuGre model," *J. Vibrat. Control*, vol. 28, nos. 19–20, pp. 2519–2530, Oct. 2022.

[17] S. Luo and R. Gao, "Chaos control of the permanent magnet synchronous motor with time-varying delay by using adaptive sliding mode control based on DSC," *J. Franklin Inst.*, vol. 355, no. 10, pp. 4147–4163, Jul. 2018.

[18] S. Luo, F. L. Lewis, Y. Song, and H. M. Ouakad, "Accelerated adaptive fuzzy optimal control of three coupled fractional-order chaotic electromechanical transducers," *IEEE Trans. Fuzzy Syst.*, vol. 29, no. 7, pp. 1701–1714, Jul. 2021.

[19] H. Wang, S. Liu, D. Wang, B. Niu, and M. Chen, "Adaptive neural tracking control of high-order nonlinear systems with quantized input," *Neurocomputing*, vol. 456, pp. 156–167, Oct. 2021.

[20] Y. Xia, J.-Y. Li, Y.-K. Song, J.-X. Wang, Y.-F. Han, and K. Xiao, "Prescribed performance-tangent barrier Lyapunov function for adaptive neural backstepping control of variable stiffness actuator with input and output constraints," *Int. J. Control, Autom. Syst.*, vol. 21, no. 3, pp. 975–992, Mar. 2023, doi: 10.1007/s12555-021-0629-4.

[21] Q. Shen, P. Shi, R. K. Agarwal, and Y. Shi, "Adaptive neural network-based filter design for nonlinear systems with multiple constraints," *IEEE Trans. Neural Netw. Learn. Syst.*, vol. 32, no. 7, pp. 3256–3261, Jul. 2021.

[22] Q. Shen, Y. Shi, R. Jia, and P. Shi, "Design on type-2 fuzzy-based distributed supervisory control with backlash-like hysteresis," *IEEE Trans. Fuzzy Syst.*, vol. 29, no. 2, pp. 252–261, Feb. 2021.

[23] Y. Song, Y. Xia, J. Wang, J. Li, C. Wang, Y. Han, and K. Xiao, "Barrier Lyapunov function-based adaptive prescribed performance control of the PMSM used in robots with full-state and input constraints," *J. Vibrat. Control*, vol. 29, nos. 5–6, pp. 1400–1416, Mar. 2023.
[24] Z. Yao, X. Liang, G.-P. Jiang, and J. Yao, "Model-based reinforcement learning control of electrohydraulic position servo systems," *IEEE/ASME Trans. Mechatronics*, vol. 28, no. 3, pp. 1446–1455, Jun. 2023.
[25] S. Gao, X. Liu, Y. Jing, and G. M. Dimirovski, "Finite-time prescribed performance control for spacecraft attitude tracking," *IEEE/ASME Trans. Mechatronics*, vol. 27, no. 5, pp. 3087–3098, Oct. 2022.
[26] H. F. Min, S. Y. Xu, and Z. Q. Zhang, "Adaptive finite-time stabilization of stochastic nonlinear systems subject to full-state constraints and input saturation," *IEEE Trans. Autom. Control*, vol. 66, no. 3, pp. 1306–1313, Mar. 2021.
[27] T. Gao, Y. Liu, L. Liu, and D. Li, "Adaptive neural network-based control for a class of nonlinear pure-feedback systems with time-varying full state constraints," *IEEE/CAA J. Autom. Sinica*, vol. 5, no. 5, pp. 923–933, Sep. 2018.
[28] R. Dhaouadi, F. H. Ghorbel, and P. S. Gandhi, "A new dynamic model of hysteresis in harmonic drives," *IEEE Trans. Ind. Electron.*, vol. 50, no. 6, pp. 1165–1171, Dec. 2003.
[29] X. Bu, X. Wu, R. Zhang, Z. Ma, and J. Huang, "Tracking differentiator design for the robust backstepping control of a flexible air-breathing hypersonic vehicle," *J. Franklin Inst.*, vol. 352, no. 4, pp. 1739–1765, Apr. 2015.
[30] Y. Tang, Y. Wu, M. Wu, X. Hu, and L. Shen, "Nonlinear tracking-differentiator for velocity determination using carrier phase measurements," *IEEE J. Sel. Topics Signal Process.*, vol. 3, no. 4, pp. 716–725, Aug. 2009.
[31] D. Tian, H. Shen, and M. Dai, "Improving the rapidity of nonlinear tracking differentiator via feedforward," *IEEE Trans. Ind. Electron.*, vol. 61, no. 7, pp. 3736–3743, Jul. 2014.

YU XIA (Graduate Student Member, IEEE) received the B.Eng. degree in mechanical engineering from Chongqing University, Chongqing, China, in 2017, where he is currently pursuing the Ph.D. degree with the State Key Laboratory of Mechanical Transmission. His research interests include variable stiffness actuator, mechanical and electrical transmission control, dynamic analysis, and adaptive control.

CHENG WANG received the M.S. degree in vehicle engineering from Chongqing University, in 2018, where he is currently pursuing the Ph.D. degree in mechanical engineering. His research interests include mechanical design, highly reliable and precise transmission and drive, bionic intelligent robot, and gear dynamics.

YANKUI SONG received the B.Eng. degree in mechanical engineering from Chongqing University, Chongqing, China, in 2017, where he is currently pursuing the Ph.D. degree with the State Key Laboratory of Mechanical Transmission. His research interests include mechanical and electrical transmission control, adaptive control, and chaos control of nonlinear systems.

JIANLIN CAI was born in 1993. He received the Ph.D. degree in mechanical engineering from Chongqing University, in 2022. His main research interests include tribological action mechanism and rotor dynamics.

GONG CHENG was born in 1993. He received the Ph.D. degree in mechanical engineering from Chongqing University, in 2022. He is currently with the Chongqing Industry Polytechnic College. His main research interests include tribo-dynamic of mechanical transmission systems, mixed lubrication theory, interface mechanics, surface bionic texture, and wear mechanism.